(2) ✓

# SINGLE CRYSTAL FIBERS OF $MgO:LiNbO_3$

## FINAL REPORT



Contract Number F49620-88-C-0084

August 7, 1990

PREPARED FOR

U. S. AIR FORCE OFFICE OF SCIENTIFIC RESEARCH
BUILDING 410
BOLLING AFB, DC 20332-6448

PRINCIPAL INVESTIGATOR: DR. RICHARD G. SCHLECHT

LASERGENICS CORPORATION
PO BOX 611330
SAN JOSE, CA 95161-1330

# SINGLE CRYSTAL FIBERS OF $MgO:LiNbO_3$

## FINAL REPORT

Contract Number F49620-88-C-0084

August 7, 1990

PREPARED FOR

U. S. AIR FORCE OFFICE OF SCIENTIFIC RESEARCH
BUILDING 410
BOLLING AFB, DC 20332-6448

PRINCIPAL INVESTIGATOR: DR. RICHARD G. SCHLECHT

LASERGENICS CORPORATION
PO BOX 611330
SAN JOSE, CA 95161-1330

Unclassified
SECURITY CLASSIFICATION OF THIS PAGE

(2)

LASERGENICS

# REPORT DOCUMENTATION PAGE

Form Approved
OMB No. 0704-0188

| | |
|---|---|
| 1a REPORT SECURITY CLASSIFICATION: (U) | 1b RESTRICTIVE MARKINGS: N/A |
| 2a SECURITY CLASSIFICATION AUTHORITY: N/A | 3 DISTRIBUTION/AVAILABILITY OF REPORT: Approved for public release; distribution unlimited. |
| 2b DECLASSIFICATION/DOWNGRADING SCHEDULE: N/A | |
| 4 PERFORMING ORGANIZATION REPORT NUMBER(S): F49620-88-C-0084 | 5 MONITORING ORGANIZATION REPORT NUMBER(S): AFOSR-TR-N/A 1189 |
| 6a NAME OF PERFORMING ORGANIZATION: LaserGenics Corp. | 6b OFFICE SYMBOL (If applicable): N/A |
| 6c ADDRESS (City, State, and ZIP Code): P. O. Box 611330, San Jose, CA 95161-1330 | 7a NAME OF MONITORING ORGANIZATION: USAF, AFSC, Air Force Office of Scientific Research |
| | 7b ADDRESS (City, State, and ZIP Code): Building 410, Bolling AFB, DC 20332-6448 |
| 8a NAME OF FUNDING/SPONSORING ORGANIZATION: USAF, AFSC | 8b OFFICE SYMBOL (If applicable): NP |
| | 9 PROCUREMENT INSTRUMENT IDENTIFICATION NUMBER: Contract # F49620-88-C-0084 |
| 8c ADDRESS (City, State, and ZIP Code): Building 410, Bolling AFB, DC 20332-6448 | 10 SOURCE OF FUNDING NUMBERS |

| PROGRAM ELEMENT NO. | PROJECT NO. | TASK NO. | WORK UNIT ACCESSION NO. |
|---|---|---|---|
| 61102F | 3005 | A1 | N/A |

DTIC ELECTE JAN 04 1991 S D

11 TITLE (Include Security Classification)

(U) Single Crystal Fibers of $MgO:LiNbO_3$

12. PERSONAL AUTHOR(S)

Dr. Richard Schlecht

| 13a TYPE OF REPORT | 13b TIME COVERED | 14. DATE OF REPORT (Year, Month, Day) | 15. PAGE COUNT |
|---|---|---|---|
| Final | FROM 6/29/88 TO 8/7/90 | 90-8-7 | 38 |

16. SUPPLEMENTARY NOTATION

| 17. COSATI CODES | | | 18. SUBJECT TERMS (Continue on reverse if necessary and identify by block number) |
|---|---|---|---|
| FIELD | GROUP | SUB-GROUP | Single Crystal Fibers, $MgO:LiNbO_3$, Nonlinear Optics Crystal Growth |
| | | | |
| | | | |

19. ABSTRACT (Continue on reverse if necessary and identify by block number)

As optical instruments and devices see a broader and wider use it becomes necessary to increase their efficiency in order to make them more compact and lighter in weight, particularly for space applications. Nonlinear optical devices, such as second harmonic generators and parametric oscillators, will be an important part of this in order to create new wavelengths and tunable sources. If these devices can be made in fiber form, a significant improvement in efficiency will result. It will then be possible to use the efficient semiconductor lasers as a pump in spite of their poor beam quility. We have investigated the growth of $Mg:LiNbO_3$ in fiber form using the laser-heated pedestal-growth technique. We were able to grow fibers of good optical quality without resorting to post-growth processing. However, we didanneal the fibers to improve their mechanical properties. Different techniques were tried to pole the fibers with limited success.

| 20 DISTRIBUTION/AVAILABILITY OF ABSTRACT | 21 ABSTRACT SECURITY CLASSIFICATION |
|---|---|
| ☐ UNCLASSIFIED/UNLIMITED ☐ SAME AS RPT ☒ DTIC USERS | (U) |

| 22a NAME OF RESPONSIBLE INDIVIDUAL | 22b TELEPHONE (Include Area Code) | 22c OFFICE SYMBOL |
|---|---|---|
| Dr Howard Schlossberg | 202/767-4906 | NP |

DD Form 1473, JUN 86 — Previous editions are obsolete.

SECURITY CLASSIFICATION OF THIS PAGE

Unclassified

TABLE OF CONTENTS





# PROJECT SUMMARY

The purpose of this research program was to expand our understanding of the growth of fibers of the nonlinear optical material, $MgO.LiNbO_3$. This material is of interest because of its large nonlinear optical coefficients and its good optical properties. The undoped material suffers from photorefractive damage. It has been found that by doping $LiNbO_3$ with approximately 5% of MgO, the phasematch temperature increases to the point that the material becomes self annealing. This makes this material particulaly attractive for second harmonic generation of infrared laser sources and for other nonlinear devices.

Second harmonic generation of laser sources using fiber materials has several important advantages. Such components could be used in integrated optical devices, significantly reducing the size of these systems. Moreover, the use of fibers for these elements can lead to important improvements in the efficiency of conversion of the laser source to the second harmonic as the guided wave will maintain collinearity over the length of the fiber. This increases the interaction length, resulting in an improved conversion efficiency. Fibers are also very easy to temperature control, an important feature for phase matched second harmonic generation.

During the course of our project we studied the growth characteristics of $MgO.LiNbO_3$. We made 18 growth runs of this material and were able to improve on the growth conditions so as to be able to grow fibers of good optical quality without resorting to post growth processing. However, the mechanical strength of the fibers were not as desired and an annealing process was required to increase the strength of the as-grown fibers. Problems were encountered when we attempted to pole the two domain a-axis fibers in order to obtain single domain fibers. Asymmetric heating and electric field poling and both techniques together were tried with out success. Control ofthe process was too critical for the system we used and several fibers were lost. The only process that appears promising to us is symmetric heating with electric field poling near the melting point of $MgO.LiNbO_3$. Further work needs to be done to evaluate the characteristics of this process in order to obtain single domain fibers of this material. Once this is achieved, highly efficient nonlinear optical devices using fibers of $MgO.LiNbO_3$ will result.

# SECTION 1

# INTRODUCTION

As spectroscopic and other optical instruments are used in a wider range of experiments and environments, such as in outer space, it becomes necessary to make these instruments smaller and more compact, lighter in weight and more efficient. The most efficient and compact laser source at this time is the semiconductor laser. This laser has achieved efficiencies of greater than 50%. However this laser has some serious limitations that do not allow its use for many scientific studies. Some of these limitations are that the beam quality of these lasers is usually poor, the beam divergence is great and the beam is astigmatic and the laser can not be tuned over a wide spectral range. However this laser is ideal as a pump source for a solid state laser that can overcome these shortcomings. A system that could be envisioned as a spectroscopic source is a semiconductor diode laser pumping a Nd:YAG laser that is frequency doubled to 532 nm. This output is then used to pump a $Ti:Al_2O_3$ laser that is continuously tunable from 660 nm to over 1000 nm. The possibility thus exists for an all fiber laser system. Fiber lasers of Nd:YAG have already operated successfully. The next step would be to develop the frequency doubler to double the output of this fiber laser to 532 nm. Significant success has already been achieved at Stanford University in the growth of single crystal fibers of $MgO:LiNbO_3$ as frequency doublers. LaserGenics has the exclusive license to the patents held by Stanford University on the laser-heated pedestal-growth (LHPG) technique for growing single crystal fibers. We have investigated the growth of $MgO:LiNbO_3$ using this technique as a function of the melt temperature and the atmosphere using source rods prepared from single crystal material grown by Crystal Technology, Inc. We also investigated the post growth anneal to minimize defects and oxygen loss in the fibers. We have made preliminary investigations of techniques to pole these fibers in order to obtain single domain a-axis fibers with limited success.

$MgO:LiNbO_3$ fibers are potentially useful in a variety of electo-optical devices that take advantage of its large piezoelectric, pyroelectric, electro-optic and nonlinear optical coefficients. Nonlinear interactions in the fiber form are attractive because the fiber eliminates beam spreading due to diffraction, thus leading to enhanced frequency conversion efficiencies. Our primary interest is in frequency doubling the 1.06 micron radiation from a fiber Nd:YAG laser. At this frequency lithium niobate will be non-critically phasematched near room temperature.[1] To obtain non-critical phasematching in the fiber, the fiber must be grown orthogonal to the c-axis. It has been found that $MgO:LiNbO_3$ will grow readily along the a-axis. Two complications

result during the growth of MgO:$LiNbO_3$ fibers. These are the oxygen loss during growth[2] and the poor mechanical strength of the fibers. Associated with the oxygen loss is a brownish coloring that the fibers exhibit, making them unsuitable for optical applications. However, it is possible that the loss of oxygen can be corrected by annealing the fibers in a wet oxygen atmosphere for eight hours at 900° C.[2,3] This annealing procedure leads to an additional benefit in that a marked improvement in the mechanical properties of the fibers results as well, presumably due to the removal of crystal strains in the fibers.

Another problem to be overcome in the development of these fibers as frequency doublers is to pole the fibers into single domains. As is typical of ferroelectric materials, as-grown crystals tend to break up into a number of regions of reversed spontaneous polarization (ferroelectric domains). Since the sign of most of the material parameters differs in antiparallel domains, the efficiency of many devices depends on the preparation of "poled" fibers, i.e. fibers containing only a single ferroelectric domain.

As-grown bulk crystals of MgO:$LiNbO_3$ tend to exhibit multi-domain structures. These domain distributions are conventionally explained in terms of a balance between depolarization energy, which favors a highly multidomain configuration, and domain wall energy, which favors a single domain crystal.[4] In c-axis rods these domains tend to take the form of concentric rings, while in a-axis rods the domains form a series of layers perpendicular to the rod axis. The domain wall spacing that minimizes the sum of the depolarization energy and the domain wall energy in an a-axis rod can be calculated. The result for the domain wall spacing, $\Omega$, as a function of the rod radius, $\rho$, is given by:

$$\Omega = \sqrt{\rho}[(\pi^3/2.10)\varepsilon_0(\varepsilon + 1)\,\sigma/P_S^2]^{1/2} \qquad 1.1$$

where $\varepsilon$ is the dielectric constant of the rod, $\sigma$ is the domain wall energy and $P_S$ is the spontaneous polarization per unit volume. Because the material properties are not well known near the Curie temperature and since the quantity in the square brackets is independent of the rod diameter it is best to estimate the domain wall spacing in the fibers by scaling the measurements in the bulk crystals by the square root of the diameter. The typical domain size for centimeter diameter bulk a-axis boules is several hundred microns. Therefore we would expect that the domain spacing in a 500 µm fiber would be of the order of 100µm.

However, it has been observed that the fibers do not break up into small domains. In fact the c-axis grown material is single domain and the a-axis fibers contain two domains that are anti-parallel with the wall perpendicular to the c-axis. These two cases are depicted in Figure 1.1. It is clear then

that for the fibers depolarization and domain wall energies are not the complete picture. Fejer[5] has determined that the thermoelectric effect can produce electric fields large enough to pole the fibers in this way during the growth process. This electric field produced by the thermoelectric effect is given by.

$$\mathbf{E} = \mathbf{Q} \cdot \nabla T$$

where **E** is the electric field, T is the temperature and **Q** is the second rank thermoelectric power tensor. Near the Curie temperature **Q** has the value of 0.8 mV/°K in MgO:$LiNbO_3$. Because of the huge temperature gradients that exist during the fiber growth process, large enough fields exist to pole the fibers as observed. For the c-axis growth case the major temperature gradient is along the c-axis so that the fiber is poled along this axis. For an a-axis growth fiber the major temperature gradient is radial and still along the c-axis. This radial dependence along the c-axis leads to the head-to-head domains observed in a-axis growth fibers.

These observations suggests a technique to pole the a-axis fibers in order to obtain a single domain fiber. By asymmetrically heating the fiber on the surface where the c-axis emerges from the fiber but not on the opposite face, this temperature gradient can cause the fiber to spontaneously pole. Another procedure would be the application of an electric field along the c-axis. The most effective poling procedure may be a combination of these techniques.

We have investigated the growth of MgO:$LiNbO_3$ in fiber form using the laser-heated pedestal-growth technique. In section 2 we discuss the theory of nonlinear effects in fibers. In section 3 we discuss the laser-heated pedestal-growth technique and why it is so attractive for growing high quality single crystal fibers and in section 4 we discuss the results.

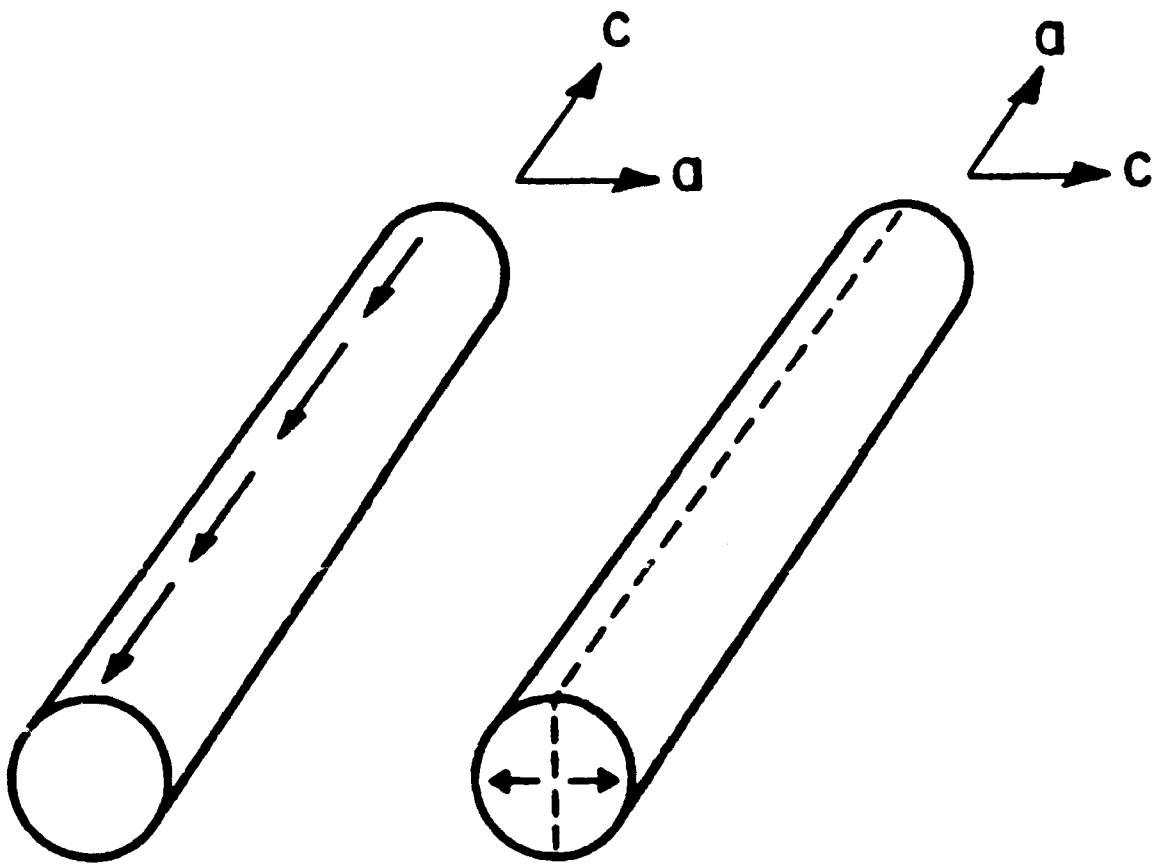


Figure 1.1. Domain distributions in $LiNbO_3$ for a-axis and c-axis fibers

## SECTION 2

## THEORY OF NONLINEAR FIBER DEVICES

In this section we will consider those effects that play an important part in determining the efficiency for second harmonic generation (SHG) in fibers. We begin by relating the well-known results of SHG in bulk materials. This was first discussed by Armstrong, Bloembergen, Ducuing and Pershan[6] in 1962 starting from Maxwell's equations. These equations can be solved in closed form for the plane wave case. A nonlinear polarization term is introduced at each of the frequencies of the waves. These nonlinear polarization terms are of the form

$$P_{NL}(\omega_i) = d_{ijk}\, E(\omega_j)\, E(\omega_k) \qquad 2.1$$

For second harmonic generation: $\omega_i = \omega_j + \omega_k$ and $\omega_j = \omega_k$ so that $\omega_i = 2\omega_j$

If it is assumed that there are no absorption or other losses, that negligible power is transferred between waves and that the amplitudes vary slowly, the wave equation can be easily integrated to give the beam intensity at the second harmonic as:

$$I(2\omega) = \omega^2 \kappa^2 d_{eff}^2 L^2 I^2(0) \operatorname{sinc}^2(\Delta kL/2) \qquad 2.2$$

where $d_{eff}$ is the effective coupling coefficient which is related to the nonlinear susceptibility and $\Delta k$ is given by

$$\Delta k = 2k_{\omega} - k_{2\omega} = 2\omega\sqrt{(\varepsilon_0\mu_0)}[n(\omega) - n(2\omega)] \qquad 2.3$$

From this we can see that the conversion efficiency increases both with the interaction length L and with the intensity I(0) of the pump beam. One would think that the conversion efficiency could be increased by focusing the pump beam to obtain a higher value of I(0). However, the effects of focusing on conversion efficiency can be determined by recalling that a Gaussian beam of wavelength $\lambda$ focused to a radius $w_0$ in a solid with refractive index n remains collimated over an approximate length $2\ell_R$, where the Rayleigh length, $\ell_R$, is given by

$$\ell_R = \pi n w_0^2/\lambda \qquad 2.4$$

Therefore, as the beam is focused with shorter and shorter focal lengths to decrease $w_0$, the interaction length, $2\ell_R$, is decreased by the square of $w_0$. With

a nonlinear interaction involving focused beams, a trade-off exists between a small focal spot and a long interaction length. For noncritically phase-matched second harmonic generation in a crystal of length L, it can be shown that optimum conversion occurs for confocal focusing, i.e., when the confocal parameter of the pump beam is approximately equal to the length of the crystal. Mathematically, if the waist of the Gaussian beam is $w_0$, then the optimum focusing condition is when

$$L = 5.68\, l_R \qquad 2.5$$

When this focusing condition is met, $\eta_B$, the conversion efficiency for bulk second harmonic generation in the undepleted pump limit, is:

$$\eta_B = I(2\omega)/I(\omega) = (2\omega)^2\sqrt{\varepsilon_0\mu_0}^3\,(d^2/2n^3)I(\omega)(1.2L/\lambda) \qquad 2.6$$

The conversion efficiency expression for guided waves has also been calculated to be given by:

$$\eta_G = I(2\omega)/I(\omega) = (2\omega)^2\sqrt{\varepsilon_0\mu_0}^3\,(d^2/2n^3)[I(\omega)/A_{eff}]L^2 \qquad 2.7$$

If we take the ratio of the guided and bulk efficiencies from Eqs. 2.6 and 2.7 we note that

$$\eta_G/\eta_B = L\lambda/(2.4\pi A_{eff}) \qquad 2.8$$

It is interesting to determine the significance of this result. We define a dimensionless effective area, $\underline{A}$, by:

$$\underline{A} = A_{eff}/(\pi\rho^2) \qquad 2.9$$

where $\rho$ is the fiber radius. Then the ratio of the guided to bulk efficiency is given by

$$\eta_G/\eta_B = (L\lambda/\rho^2)(2.4\pi\underline{A})^{-1} \qquad 2.10$$

From this we can see that, for a given radius, the relative efficiency of the guided wave interaction increases with both L and $\lambda$, as one would expect as the importance of diffraction also increases with both L and $\lambda$. The improvement in efficiency can be substantial. If we let L=10cm, $\lambda$ = 1μm, $\rho$=25μm, n=2, $\underline{A}$=1/2,

then $\eta_G/\eta_B \approx 40$. We have developed this for second harmonic generation but one would expect similar improvements for other nonlinear interactions. For interactions involving widely separated frequencies, even larger improvements are to be expected because of the relatively poor overlap for bulk interactions.

For a 10cm-long piece of lithium niobate, the efficiency for bulk confocal second harmonic generation at 532nm is 4%/W. In a fiber with the same parameters, the conversion efficiency would be .16%/mW. At this level, one could efficiently double weak CW sources, e.g., 4mW of green light could be obtained from a 50 mW infrared source. The gain for a parametric oscillator operated at degeneracy is equal to the harmonic conversion efficiency, thus milliwatt thresholds for such devices would seem possible as well.

In our analysis to this point, we have assumed that the interaction is noncritically phasematched, and that the fiber interaction is between fundamental modes with the crystal axes aligned with the fiber axes. In critically phasematched bulk interactions, the Poynting vector walkoff limits the minimum useful spot size for a given length of crystal. This severely limits the conversion efficiency and decreases the quality of the output beam. In fibers, walkoff effects do not occur, and therefore fibers have an additional advantage over bulk interactions, although fibers whose axes are not aligned with the crystal axes may suffer leakage losses.

Clearly, single crystal fibers hold great promise for efficient low power nonlinear interactions. The discussion to this point has been confined to perfect waveguides with no axial variations. We will at this time briefly discuss these variations and the limitations they impose on nonlinear interactions and on the effects of ferro electric domains.

a. Phasematching Effects

The efficiency of nonlinear interactions depends critically on the phase mismatch, $\Delta k$. Deviations in $\Delta k$ from its nominal value ( $\Delta k=0$ for a phasematched interaction) can be caused by axial variations in both material composition and fiber cross-section. The effect of $\Delta k$ variations are now analyzed and related to diameter control tolerances.

The analysis begins with the equation for the evolution of the amplitude of the second harmonic mode

$$da/dz = \kappa \exp(-i\Delta k z) \qquad (11)$$

where $\kappa$ is the coupling constant, and $a(z)$ is the modal amplitude. We now assume an axially varying $\Delta k = \Delta k(z)$. The formal solution is straightforward

$$a(z) = \kappa \int \exp(-i\Delta k(z')z')dz' \qquad (12)$$

where we have assumed that a(0)=0, i.e., that there is no second harmonic input at the end of the fiber.

If $\Delta k$ is sufficiently large that the accumulated phase difference becomes larger than $\pi$, the second harmonic amplitude is not a monotonically increasing function of z, and the efficiency of the interaction is severely degraded. In the other limit where $\Delta k$ is small, the accumulated phase difference remains small compared to $\pi$, and the second harmonic amplitude increases monotonically, but more slowly than for a perfectly phasematched interaction.

If the accumulated phase shift is small compared to $\pi$, we can apply a perturbation approach and expand the exponential in a power series, so that:

$$a(L) = K[L + iI_1(L) - 1/2 I_2(L)] \qquad 2.13$$

where L is the length of the fiber, and:

$$I_1(L) = \int \Delta k(z')z'dz' \qquad 2.14$$

$$I_2(L) = \int [\Delta k(z')z']^2 dz' \qquad 2.15$$

Assuming that $\Delta k(z)$ is random with zero mean and an autocorrelation length short compared to L, we can integrate by parts equations 2.14 and 2.15 to obtain:

$$I_1(L) = L^2\langle\Delta k\rangle/2 = 0 \qquad 2.16$$

$$I_2(L) = L^3\langle\Delta k^2\rangle/3 \qquad 2.17$$

where Eq. 2.16 follows from the assumption that $\Delta k$ has a zero mean. We can now see that the second harmonic power $P_2$ is given by:

$$P_2 \alpha a(L)^2 = K^2L^2[1 - (\langle\Delta k^2\rangle/3)L^2] \qquad 2.18$$

We now see that the second harmonic power is reduced by $(\langle\Delta k^2\rangle/3)L^2$ with respect to a perfectly phasematched interaction. Therefore, if we set our quality criterion by the requirement that the power decrease be no more than one-half with respect to a perfect interaction, then we must have:

$$\langle\Delta k^2\rangle < (3/2)L^{-2} \qquad 2.19$$

We can relate this condition to one on the fiber diameter. Let $\delta\rho$ be the RMS deviation of the fiber diameter from its mean value, i.e., $\delta\rho \equiv \sqrt{\langle\rho^2\rangle}$. Then for

small $\delta\rho$, we have:

$$\delta\rho < \sqrt{(3/2)}\,(L\partial\Delta k/\partial\rho)^{-1} \qquad 2.20$$

For fundamental mode interactions in far from cutoff step profile fibers, we have that:

$$\delta\rho/\rho < (2\pi/\sqrt{3})n_0(j_{01})^{-2}\,\rho^2/(L\lambda) \qquad 2.21$$

where $j_{01}$ is given by $j_{01} = 3\pi/4$.

For second harmonic generation with a fundamental wavelength $\lambda$ = 1 μm in a 10 cm-long, 25 μm radius fiber, we find $\delta\rho/\rho$ < 0.7% and it is <7% for a 1 cm-long fiber.

In the large accumulated phase difference limit, the decrease in efficiency depends in detail on the form of $\Delta k(z)$. As one might expect, the second harmonic power is reduced by a factor on the order $m^{-2}$ where the accumulated phase difference is $\approx m\pi$.

b. Guided Mode-Guided Mode Coupling

The modes in a fiber in general have been determined under the assumption that the waveguide was z-invariant. In fibers with axial variations in $\boldsymbol{\varepsilon}$, i.e., where $\boldsymbol{\varepsilon}(x,y,z)$, these modes no longer satisfy Maxwell's equations, and corrected solutions must be found. The usual approach to this problem is to find solutions in terms of a sum over a complete set of modes, where z-dependent amplitude coefficients represent the effects of the axial variations in $\boldsymbol{\varepsilon}$. To simplify this problem, we assume that the waveguide is isotropic, so that $\boldsymbol{\varepsilon}=n^2\mathbf{I}$.

The concept of mode coupling is covered in Ref. 7. The approach of local mode expansion is used to solve this problem. At each z, the local mode is a solution to a hypothetical z-independent waveguide whose transverse refractive index profile is the same as that of the perturbed waveguide at that value of z. These z-dependent modes are not solutions to Maxwell's equations, and therefore the true solutions must be expressed again as a sum over the local modes with z-dependent amplitude coefficients that reflect the effects of the perturbation. The advantage of the local normal modes for problems involving large perturbations is that they are discontinuous at the same radius as the actual solution.

The theory of coupled local modes is developed in Ref. 7 and it is shown there that Maxwell's equations in the perturbed waveguide can be rewritten in the form of a set of coupled equations for the modal amplitudes. The total electric field is expressed by the expansion:

$$\mathbf{E}_t(x,y,z) = \Sigma\, C_\beta(z)\mathbf{e}_t(x,y)\exp(ik_\beta z) \qquad 2.22$$

The evolution of the modal amplitudes is described by.

$$dC_\mu/dz = \Sigma R_{\mu\beta}(z)g(z)C_\beta \exp[i(k_\beta - k_\mu)z] \qquad 2.23$$

We may take k equal to the conventional definition of k. $R_{\mu\beta}$ represents the strength of the coupling, while g(z) is related to f(z), the axial dependence of the perturbation by:

$$g(z) = -i df/dz\,[1/(k_\beta - k_\mu)] \qquad 2.24$$

If we launch a single mode, say ß, into a fiber of length L and we further assume that the perturbations are sufficiently weak that only a small fraction of the incident power is scattered into other modes, then we can assume that to first order, $C_\beta(L) = C_\beta(0)$. Eq. 2.23 can be easily integrated to find the coefficients of the other modes:

$$C_\mu(L) = R_{\mu\beta}\, C_\beta(0) \int g(z) \exp[i(k_\beta - k_\mu)z]dz \qquad 2.25$$

integrating this equation once by parts and assuming that the perturbation vanishes at 0 and L, we find:

$$C_\mu(L) = R_{\mu\beta}\, C_\beta(0)\sqrt{L}\, F(k_\beta - k_\mu) \qquad 2.26$$

where F(k) is the Fourier transform of the perturbation function f(z)

$$F(k) = (1/\sqrt{L}) \int f(z) \exp(ikz)dz \qquad 2.27$$

We then find that the ratio of the power carried by each mode is given by:

$$P_\mu(L)/P_\beta(0) = |R_{\mu\beta}|^2 F(k_\beta - k_\mu)^2 L \qquad 2.28$$

Clearly, strong coupling occurs only when the Fourier spectrum of the perturbation contains components at the difference frequency of the coupled modes. We can express a periodic perturbation as having the form:

$$f(z) = \sin(2\pi z/\Lambda) \qquad 2.29$$

We define a quality criteria for perturbations as the loss over a length L of less than a fraction ε of the power incident on the waveguide. For a resonant periodic perturbation, we have that:

$$|R_{\mu\beta}|^2 < 4\varepsilon/L^2 \qquad 2.30$$

If we assume the coupling to be due to pure diameter variations on a step profile fiber and that the mode is far from cutoff, we can calculate the tolerance for coupling from an $HE_{11}$ mode to an $HE_{1m}$ mode as:

$$\delta\rho/\rho < [1.7/(m-0.25)][n_c/h(\Delta)](\rho^2/L\lambda)\sqrt{\varepsilon} \qquad 2.31$$

For $\lambda$=1μm, $\rho$=10μm, $n_c$=2 and L=1cm, we have that:

$$\delta\rho/\rho < 0.034\sqrt{\varepsilon}/[(m-0.25)h(\Delta)] \qquad 2.32$$

where $h(\Delta)$ varies between 1 for weakly guiding fibers to roughly 5 for unclad fibers. If we take $\varepsilon$=0.01, i.e., 1% loss in 1 cm, we find that for clad fibers, the diameter variations must be smaller than several tenths of a percent for coupling to the $HE_{12}$ mode, and smaller roughly as 1/m for coupling to higher order $HE_{1m}$ modes. It is also useful to know the scale of perturbation that causes coupling from the $HE_{11}$ mode to the $HE_{1m}$ mode. The resonance condition for far from the cutoff modes is given by:

$$\Lambda = 8n_c/[(m-0.25)^2 - (0.75)^2](\rho^2/\lambda) \qquad 2.33$$

With the same numerical parameters used in Eq. 2.32, we find.

$$\Lambda(\mu m) = 1600/[(m-0.25)^2 - (0.75)^2] \qquad 2.34$$

For the $HE_{12}$ mode, we find $\Lambda$ = 600μm, and the resonant wavelength decreases roughly as $1/m^2$ for coupling to higher order $HE_{1m}$ modes.

While this model is crude, it can serve as an aid in correlating experimental data. We note in passing that $\lambda^{-1}$ loss scaling was, in fact, observed in measurements of radiation losses of sapphire fibers. At Stanford, it was also observed that losses in diameter controlled fibers were not improved over those in good quality open loop fibers of the same diameter, despite a several-fold reduction in the RMS deviation. This unexpected situation can be explained by the increased spatial frequency observed for the perturbations in the closed loop fibers, and the $\Lambda^{-2}$ scaling of the loss. To completely explain this question, quantitative power spectra must be determined, but the implications of this simple model can be useful in interpreting any data.

c. Radiation Losses

The other important loss mechanism caused by structural perturbations is the coupling from the desired guided mode to the radiation modes. Calculation of these radiation losses is much more difficult than for guided mode losses. The most common approach is a coupled mode analysis. For weakly guiding fibers, the coupling coefficients are considerably more complicated than those for guided modes. For unclad fibers, one must calculate coupling coefficients from the exact radiation modes of a cylinder with arbitrary discontinuities in the dielectric constant. With the exception of the TE modes, this analysis is extremely complex and has been accomplished only for these and the $HE_{11}$ modes[8-10]. For large core-cladding index differences, other approximations have been applied, including ray tracing approaches[11,12], Fokker-Planck diffusion-like equations[13,14] and analogies to bulk scattering[15-17]. Induced current representations[12] have also been used. Finally, radiation losses caused by perturbations with too narrow a power spectrum to couple directly to radiation modes have been analyzed in terms of the statistical probability that a particular guided mode falls into the cutoff regime.[18]

We confine our discussion to qualitative comments based on the literature results for radiation losses. From the synchronicity condition, it is clear that radiation mode coupling is mediated by components ofthe perturbation that are shorter than those causing guided mode coupling. It has been shown that in planar waveguides with random, exponentially autocorrelated perturbations, for both large and small index differences, when fewer than three modes are below cutoff, the peak loss of the fundamental mode is dominated by radiation losses, while for three guided modes the peak loss is dominated by coupling to guided modes. Since the loss results are generally similar for fibers and slab waveguides[7,9], it is reasonable to expect that losses for multimoded fibers are dominated by modal scattering rather than radiation losses. Thus, we may assume that the diameter tolerances derived assuming only guided mode losses are adequate, unless the perturbation power spectrum is very wide, which has not been observed.

d. Ferroelectric Domains

As is typical of ferroelectric materials, as-grown crystals tend to break up into a number of regions of reversed spontaneous polarization (ferroelectric domains). Since the sign of most of the material parameters differs in antiparallel domains, the efficiency of devices depends on the preparation of "poled" fibers.

As-grown bulk crystals of $LiNbO_3$ tend to exhibit multi-domain structures. These domain distributions are conventionally explained in terms of a balance depolarization energy, which favors a single domain crystal[4]. In c-axis rods,

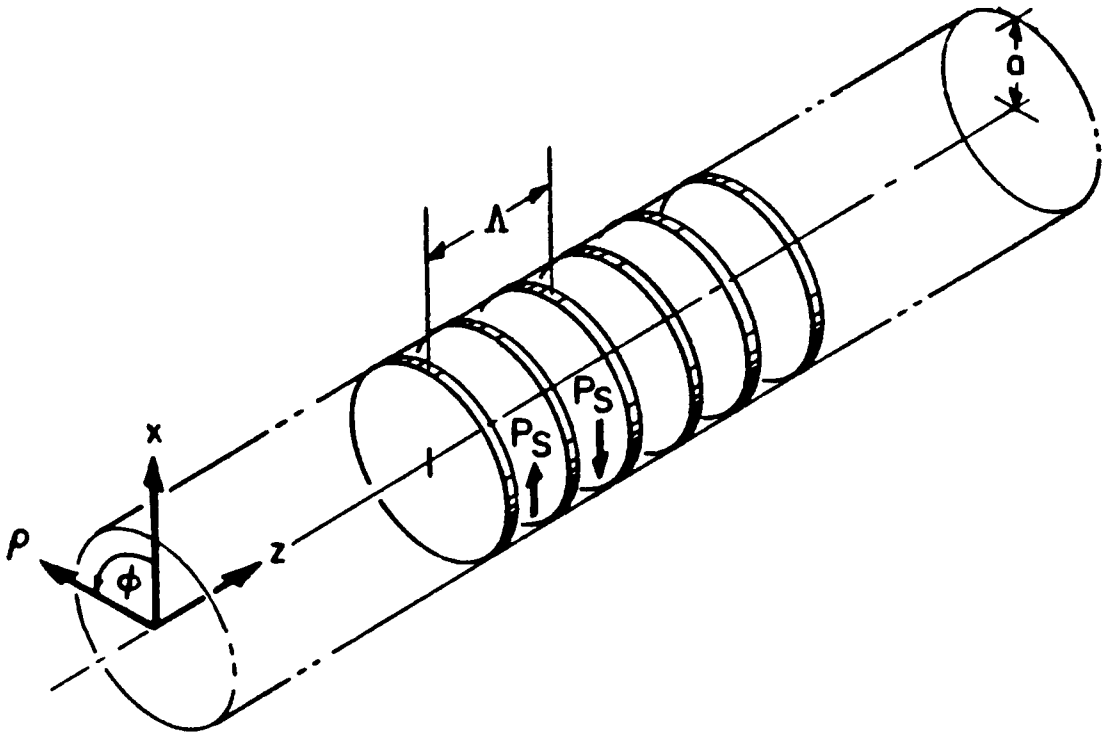


Figure 2.1. Geometry of the domain spacing in a ferro-electric fiber

between these domains tend to take the form of concentric rings, while in a-axis rods the domains form a series of layers perpendicular to the rod axis. The domain wall spacing that minimizes the sum of the depolarization energy and the domain wall energy in an a-axis rod has been calculated by M. Fejer. The geometry considered is shown in Fig. 2.1. The result for the domain wall spacing, $\Lambda$, as a function of the rod radius, a, is found to be:

$$\Lambda = \sqrt{a}[(\pi^3/2\ 10)\varepsilon_0(\varepsilon + 1)\sigma/P_S^2]^{1/2} \qquad 2.35$$

where $\varepsilon$ is the dielectric constant of the rod, $\sigma$ is the domain wall energy, and $P_S$ is the spontaneous polarization per unit volume. Since these material properties are not well known near the Curie temperature, we can best estimate the predicted domain wall spacing in fibers by noting that the quantity in square brackets is independent of rod diameter, and simply scaling the known spacing in bulk crystals by the square root of the diameter. Typical domain size for centimeter diameter bulk a-axis boules is several hundred microns. We might thus expect domain spacing of 50-100μm in 500μm diameter fibers.

Fejer measured the domain distribution in $LiNbO_3$ fibers by measuring the change in the sign of the pyroelectric coefficient in antiparallel domains. The voltage developed between a fine wire on one side of the crystal and a ground plane on the other side of the crystal was monitored while the surface of the fiber was heated with a chopped $CO_2$ laser beam. The relative phase between the chopper and the voltage across the crystal was taken as an indication of the sign of the pyroelectric coefficient, and thus of the orientation of the domain. The distribution of domains along the axis could then be measured by sliding the wire along the fiber. This technique clearly is most applicable to fibers whose axis is normal to the c-asix, and depends on an assumption that the domains are uniform along the c-axis. This assumption seemed reasonable in terms of the energy argument presented above, as head-to-head domains are a higher energy configuration than no domains at all. They were surprised when the phase of the voltage produced by an a-axis fiber was found to be independent of the position along the axis, and invariant under a 180° rotation of the fiber. The latter observation suggested that head-to-head domains were forming along the c-axis, while the former suggested that the fiber did not break up into thelayered domain structure characteristic of bulk crystals. The results for the fibers to be essentially similar to those in the bulk, they at first attributed these results to experimental error. However, these measurements were verified both with a piezoelectric technique, and a more sophisticated pyroelectric apparatus[19]. The pyroelectric device is capable of mapping out the domain distribution across the face of a fiber. They found that a-axis fibers did, in fact, break up into head-to-head domains, with the domain wall roughly at the fiber axis. These results for a-axis fibers were further verified by

etching studies by Nightingale.[20] Luh made a series of careful etching studies of both a- and c-axis fibers.[21] He again found the same results for a-axis fibers, and discovered that c-axis fibers up to 800μm in diameter were single domain. The positive c-axis of the fiber was always found to point towards the melt, independent of seed orientation.

It is clear that simple energy considerations, including only depolarization and domain wall energy, are unable to account for these empirical results. Other energy terms that affect the domain distribution must be considered. It is known that the spontaneous polarization in ferroelectrics tends to align with externally applied electric fields. At temperatures near the melting point, fields as small as 0.4V/cm applied along the c-axis of bulk crystals have been found to yield a poled, single domain structure.[22] Thus, the domains observed in crystal fibers could be explained by an internally generated electric field. A mechanism for the generation of such fields, the thermoelectric effect, exists and can serve as the basis for a model that explains all observations as shown by Fejer.

The electric field generated by carriers diffusing in the influence of a thermal gradient can be written in the form:

$$\mathbf{E} = \mathbf{Q} \cdot \nabla T \qquad 2.36$$

where **E** is the electric field, T is the tempeature, and **Q** is the second rank thermoelectric power tensor. For our purposes, it is adequate to assume that Q is isotropic and of magnitude Q. Measurement of Q in a bulk sample of congruent $LiNbO_3$ in air at temperatures close to the Curie temperature yielded a value of 0.8mV/K.[21]

Consider now the growth of a c-axis fiber. For our condition of fiber growth, the temperature gradient along the axis of the fiber can be estimated conservatively as greater than 1000 K/cm. Using Eq. 2.36, we can determine an axial electric field larger than 1 V/cm, greater than that needed to pole bulk crystals. Further, the orientation of the electric field in independent of the orientationof the seed crystal, which explains the preferred orientation of the domains in c-axis fibers. In a-axis fibers, the radial temperature gradients lead to a radial electric field. The projection of the electric field on the c-axis is then of precisely the form necessary to explain the head-to-head domains observed in a-axis fibers.

The model was further tested by heating an a-axis fiber asymmetrically to shift the temperature gradient from a symmetric to an asymmetric position with respect to the fiber axis. The position of the domain wall was found to move away from the center of the fiber, as predicted by the thermoelectric model.[21]

As pointed out previously, it is desirable from a device standpoint to use single-domain fibers. As mentioned, the as-grown c-axis fibers fortuitously

take this form. The results of the asymmetric heating experiments just described suggest an approach to poling an a-axis fiber. It is clear from the thermoelectric poling model that the direction of the spontaneous polarization in a-axis fibers is dictated by the sign of the transverse temperature gradient.

## Section 3

## LASER HEATED PEDESTAL GROWTH TECHNIQUE

It is clear from the discussion given earlier that the growth of crystal fibers of high melting point materials must overcome several difficult challenges in order to be useful for the many applications listed. A number of techniques have been used to produce single crystal fibers and these are schematically illustrated in Figure 3.1.

In the hot rolling process, shown in Figure 3.1 (a), a rod is extruded through a series of progressively smaller wire dies to produce a fiber of reduced diameter.[23] The method is primarily applicable to relatively soft materials with low melting points, e.g. alkali halides.

In the capillary-Bridgeman approach, Figure 3.1(b), a glass capillary tube is immersed in a melt of the crystal to be grown. The apparatus is slowly lowered through a temperature gradient to produce a crystalline core inside the glass tube.[24] Capillary-Bridgeman growth has primarily been applied to low-melting point organic crystals, as thermal expansion matching and chemical compatibility are critical requirements in this technique.

A number of techniques, for example the edge-defined film-fed growth and related processes, involve feeding the melt through a capillary to a die, which serves to shape the resulting fiber[25], Figure 3.1(c). These methods are reviewed in reference 26. Single crystal fibers of silver and thallium halides have been produced by such techniques[27,28], as have lower quality fibers of high melting point oxides such as sapphire, lithium niobate and spinel.[25] Particularly for high melting point materials, the choice of appropriate die material is crucial to minimize contamination of the melt and provide proper wetting conditions for stable growth. For sapphire growth with such a high melting point, this technique leads to in-diffusion of the die metal such as molybdenum.

Laser-heated pedestal growth (LHPG), illustrated in Figure 3.1(d), uses a focussed laser beam to melt the tip of a solid rod of the material to be grown. A seed crystal is dipped into the melt, then withdrawn at a faster rate than the source rod is fed in, resulting in the growth of a fiber of reduced diameter. This approach has the advantages of eliminating any possibility of crucible contamination and of achieving melt temperatures limited only by the available laser power. Moreover, difficulties in the stabilization of the fiber diameter have in large part been solved. LHPG has been applied primarily to refractory oxide materials[29-31], though halides, borides, and elemental semiconductors have also been grown.[32]

No one of these approaches is best suited to the production of high quality fibers in all materials. We have focused on the refractory oxide materials, for which LHPG offers great flexibility and has the potential to produce the purest fibers.

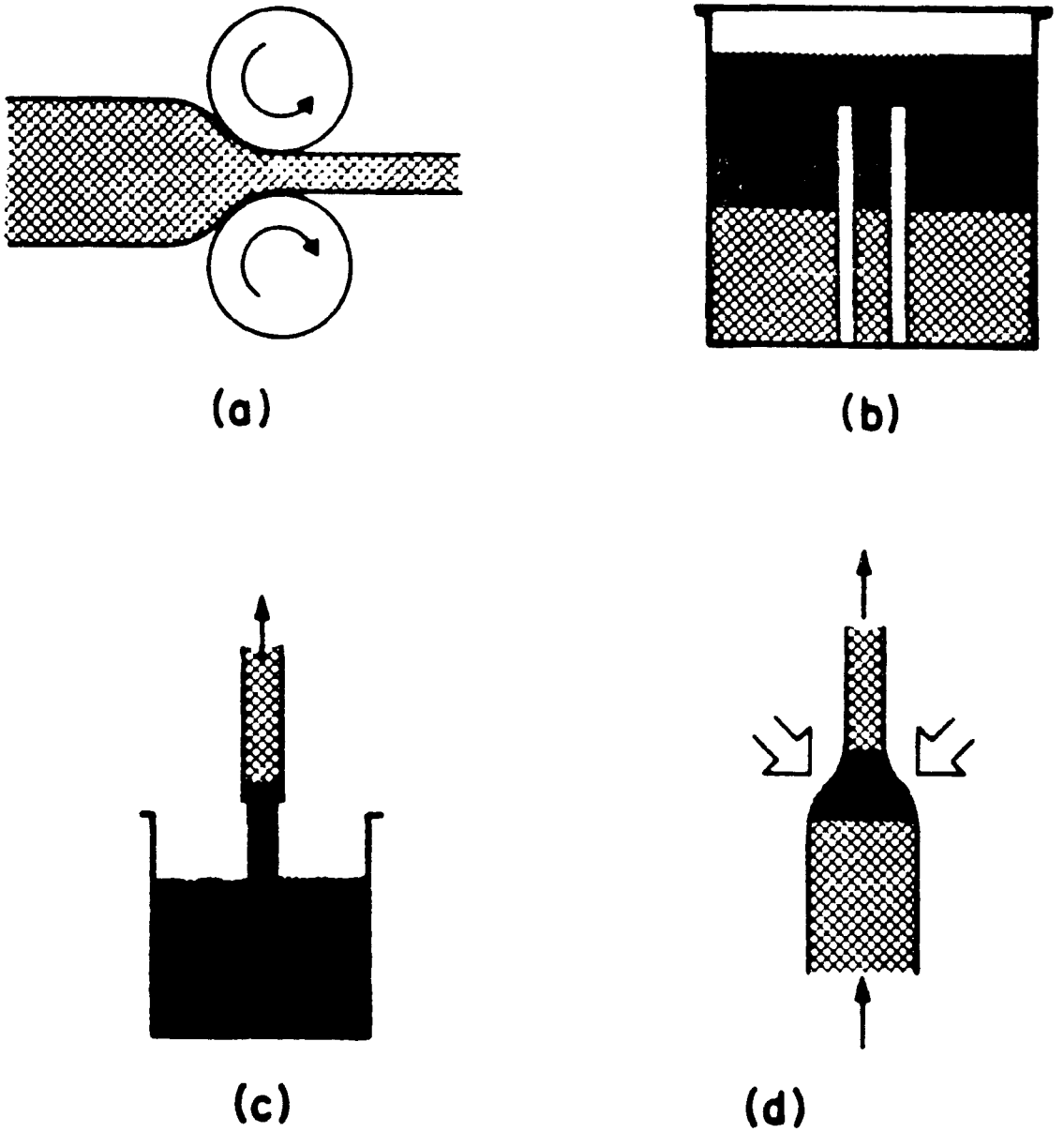


Figure 3.1. Techniques for the growth of single crystal fibers. (a) hot rolling; b) Bridgeman growth in glass capillaries; (c) edge-defined film-fed growth; (d) laser-heated pedestal-growth (LHPG)

As mentioned earlier, the LHPG technique involves melting the tip of a source rod with a focussed laser beam, dipping in an oriented seed crystal, then pulling a fiber while feeding in the source rod. This process, quite simple in principle, has several attractive features from a materials processing standpoint.

(1) Very high temperatures can be achieved, limited in principle only by the radiation temperature of the laser, and in practice by the available laser power. Only a few watts of absorbed laser power are necessary to raise the temperature of 500 μm diameter rods of typical oxide materials to their melting point.

(2) The temperature gradients at the freezing interface are on the order of thousands of degrees per cm. These large temperature gradients, in turn, allow stable growth at rates orders of magnitude larger than in bulk crystals, typically 0.1-20mm/min. As thermal stresses in a surface cooled cylinder scale with the radius, these large gradients do not lead to a cracking problem in small diameter fibers.

(3) The process is entirely crucibleless, minimizing the incorporation of undesired dopants, and facilitating the growth of a variety of materials in the same apparatus with a high degree of purity equal to the purity of the starting material.

(4) It is theoretically predicted that in the absence of phase separation or volatilization, the composition of the source rod and the fiber should be identical, so that the effective distribution coefficient approaches unity[32-34], which is particularly important in the growth of compositionally uniform solid-solution crystals. The prediction that convection in the molten zone is not oscillatory further reduces the probability of compositional striations.

In order to take advantage of these features of the LHPG process to produce fibers of high melting point materials, stable growth conditions must be realized, which in turn requires thermal and mechanical stability of the growth zone, and symmetric heat input from the laser. The heat should be delivered to a spot whose size is comparable to the source rod diameter, to produce the short molten zones necessary for stable growth. The apparatus designed to meet these requirements is now described.

A block diagram of our fiber growth apparatus is shown in Figure 3.2. A focused $CO_2$ laser melts a surface tension supported liquid zone which bridges the source and seed rods. Growth proceeds by simultaneous upward translation of the seed and source rods with the molten zone positioned between them. The laser focal spot, and consequently the molten zone, remain fixed during fiber growth. The source rod to fiber diameter ratio is set by mass conservation to be the square root of the fiber to source rod translation rate.

In order to achieve a constant fiber diameter, stable fiber growth

conditions must be realized. This in turn dictates a rigid mechanical apparatus, smooth source feed and fiber pull rates, stable laser power, and symmetric heat input into the molten zone. The LHPG apparatus utilizes novel optical and mechanical systems to achieve stable growth conditions and a uniform diameter fiber. Descriptions of the fiber growth apparatus sub-systems are given below.

A polarized $CO_2$ laser serves as the heat source for crystal growth. The water cooled laser cavity is temperature stabilized and produces a polarized $HE_{11}$ output mode with power fluctuations of less than 0.75%. A polarization power control system is used to adjust the laser power incident on the molten zone. After passing through a ZnSe beam expanding telescope and some beam steering optics the $CO_2$ beam enters the controlled atmosphere growth chamber.

Within the growth chamber a novel optical system focuses the laser beam onto the fiber with a 360 degree axially symmetric distribution as shown in Figure 3.3. The symmetric irradiance prevents cold spots in the growth zone and represents a significant improvement over the previously used two beam[35] rotating periscope,[36] or ellipsoidal[37] focusing systems.

A novel optical element incorporated into the design is a reflexicon[38] which consists of an inner cone surrounded by a larger coaxial cone. In order to achieve good optical performance it is critical that the reflexicon's two cones be accurately aligned. A mated surface design using diamond turned copper optical components, assures centering of the cone's axes. A gold coating on the copper optical surfaces enhances reflectivity and protects the copper substrate. The reflexicon and parabolic mirror provide near diffraction limited f/2 focusing, yielding a minimum spot size of 30 microns. This tight focus is important for the stable growth of small diameter fibers. The focal spot size can be controlled by modifying the input beam divergence with the focusing telescope. X-Y stages on the fiber and source rod translation devices permit adjustment of the fiber position with respect to the fixed laser focal spot.

Fiber translation speed is controlled by a phase-locked control circuit which enables d.c. motor operation over a 250,000:1 speed range with acquisition times of 1 ms. A useful control option allows the pull-to-feed translation ratio to be fixed while adjusting the growth speed. Since starting transients exist during initiation of fiber growth, a slow growth rate allows time for adjustments. As the equilibrium growth conditions are reached, the growth speed can be increased without affecting the fiber diameter.

The first step in the growth of a fiber is the preparation of the source material. The requirements on the source rod are: (1) it should have the composition of the desired end product (assuming that no volatilization takes place during growth), (2) it should have constant density, and have as close to theoretical density as possible, (3) the cross-section should be constant, as

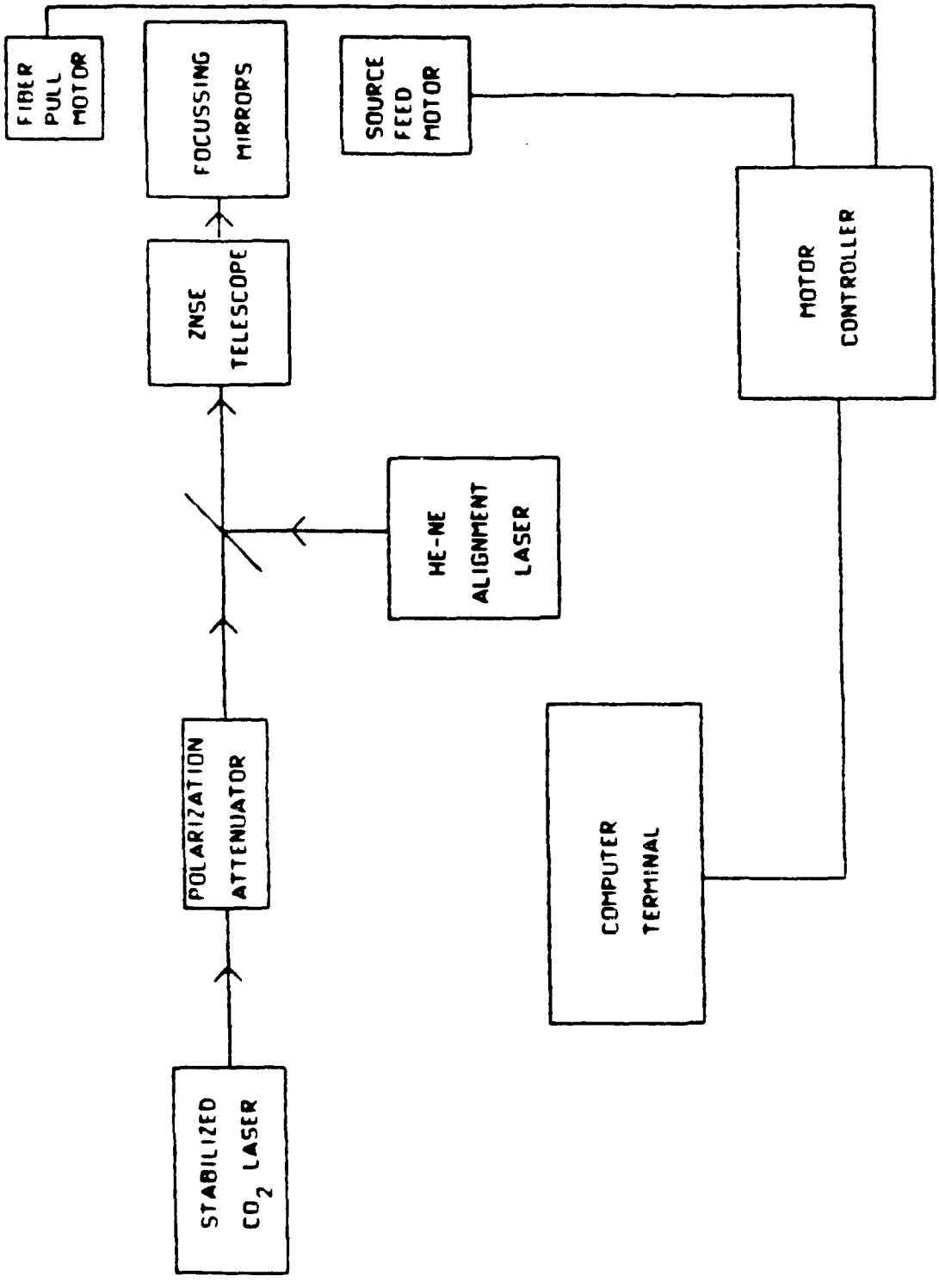


Figure 3.2. Block diagram of the LHPG apparatus.

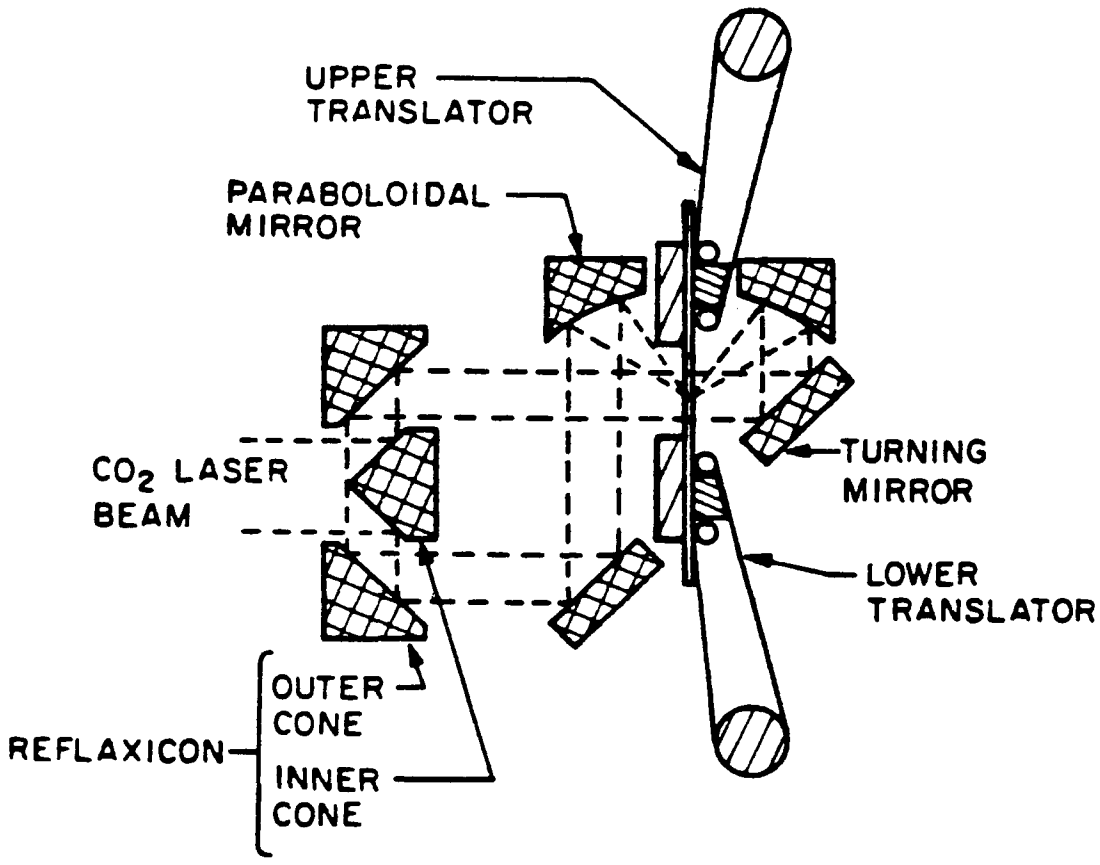


Figure 3.3. Cross-section of the growth head, showing the reflexicon focussing system and the fiber translation mechanisms. The optical elements are rotationally symmetric about their centerline.

small as possible, and preferably circular. We have had good success using a centerless grinder to fabricate starting rods with diameters as small as 300 μm and tapers as small as 1 μm/cm. The rod material itself can be a single crystal obtained elsewhere, a polycrystalline source material from solidified melts, a cold-pressed and sintered powder, or a hot-pressed powder. All of these have been used successfully.[20,39,40]

The next step in the growth is to melt the tip of the source rod with the $CO_2$ laser beam, and to dip in a seed crystal. The seed can be an oriented centerless-ground rod, a previously grown fiber or, in the case of a first growth, a platinum wire or a fiber of a higher melting point material. Because of the symmetrical heat input of the reflexicon focussing system, the azimuthal orientation of the seed has no direct effect on the growth.

After the seed is oriented, the laser power is adjusted to produce the desired length of molten zone. The molten zone must also be adjusted to produce the proper contact angle between the melt and the seed.

Growth is initiated at this point by simply simultaneously switching on the pull and feed motors, which have previously been set to run at the appropriate speeds. Lengths over 100 cm have been grown to date. In principle, lengths of fiber are limited only by the available feed material. This latter limitation is not serious in practice, in that each centimeter length of 1.25 mm diameter feed material could produce 5 meters of 50 μm diameter fiber if processed three times.

Only a modest amount of power is necessary to produce an appropriate molten zone. For example, 2 watts incident power is adequate for the growth of a 170μm diameter sapphire fiber from a 500μm diameter source rod. Typical growth rates are 0.1-20 mm/min, several orders of magnitude faster than is typical of bulk crystal growth. The mechanism that limits the maximum possible growth rate appears to vary for different materials. In Reference 20, Nightingale shows that for sapphire grown at rates faster than 8 mm/min, constitutional supercooling with respect to an unknown species, possibly Al or $O_2$ leads to the formation of microvoids along the axis of the fiber that cause severe optical scattering problems. Growth in a He atmosphere to increase the thermal gradients at the interface may lead to higher useful growth rates.

We have generally found it possible to grow fibers approximately a factor of three smaller in diameter than the source rod for growth in air. As the diameter reduction is increased, the damping coefficient for diameter variation decreases, eventually becoming negative at a critical diameter reduction $R_c$. Growth at diameter reductions larger than $R_c$ is thus unstable. For $Al_2O_3$ this instability occurs at a reduction between 3 and 4 when grown in air. It is possible that diameter reductions between 4 and 5 could be achieved when grown in a helium atmosphere.

LaserGenics Corporation has recently obtained the exclusive rights to the

three patents held by Stanford University on this single crystal fiber growth process using the LHPG technique. We are developing this process in order to obtain high quality single crystal fibers of several meter lengths. The LHPG technique is an excellent method to grow single crystal fibers. It is likely that for many high melting point materials no other technique will be able to grow similarly good quality single crystal fibers.

With this process, the atmosphere can be accurately controlled during growth as well as the crystal growth temperature. Because of the steep thermal gradients in the growth zone with this technique, the crystal structure that is "frozen in" can to some degree be controlled. We feel that this is an ideal technique to investigate the growth of high melting point materials. This technique is closely related to the float-zone method which is the best known technique to grow incongruently melting compositions.

## SECTION 4

## RESULTS AND CONCLUSIONS

In this section we will first review the results that have been obtained at Stanford University. The purpose is to inform the reader of the earlier results and to demonstrate that the theory described earlier is indeed valid. These results have been obtained primarily by Dr. Marty Fejer, Dr. John Nightingale and others of the Stanford group. Most of these results have been obtained on sapphire and YAG fibers, however, they do validate the theory presented. Following this discription we will present our results on the growth of MgO:$LiNbO_3$ fibers.

As remarked earlier, the optical performance of devices made of single-crystal fibers is controlled in large part by the scatter losses. As we noted earlier, three types of losses are important in single-crystal fibers: guided mode coupling, radiation losses, and material absorption. The latter two are readily measured by integrating sphere and calorimetric techniques, respectively, but the guided mode coupling is far more difficult to quantify. Unfortunately, the guided mode coupling is also expected to be the largest component of the total losses. It is therefore important to obtain at least an estimate of the guided mode loss.

a. Guided-Mode Coupling

The sketchy available data are the result of measurements made by Digonnet and Gaeta on single-crystal Nd:YAG fiber lasers, given in Ref. 41. They made lasers in both open-loop and closed-loop fibers, where the closed-loop fibers were grown under feedback control and typically showed 0.5% RMS diameter variations, while the open loop fibers were grown without the benefit of feedback control, and typically had 2% RMS diameter variations. Quantitative power spectra of the diameter variations are not available for these fibers, so both these amplitudes and their estimated autocorrelation length of 10 x (fiber radius) should be regarded as approximate. Both clad and unclad fibers were used, where the clad fibers were extrusion coated with LaSF30 glass, leading to a core-cladding index of refraction difference of 0.048.

The data can be summarized as follows: For a series of unclad open loop fibers with diameters ranging between 75 and 225μm, the loss scaled approximately as $\rho^{-3/2}$, where $\rho$ is the fiber radius. If the loss is expressed in $cm^{-1}$ and the fiber radius in cm, the following expression is a good fit to the data:

$$\alpha = C\rho^{-3/2} \qquad 4.1$$

where $C \approx 1.25 \times 10^{-4}\ cm^{1/2}$, though there is considerable scatter in the data. The loss of an unclad closed loop fiber of 48μm diameter was measured as $0.06cm^{-1}$, while a 41 μm diameter clad open-loop fiber had $0.02cm^{-1}$ loss.

To compare these results with theoretical predictions, consider Fig 4.1 which plots the normalized loss for unclad Nd:YAG fibers vs. the normalized autocorrelation length $D/\rho$, using a profile height of $\Delta=0.35$ and an autocorrelation decay exponent $s=3$. The precise choice of s does not greatly affect the results for the cases discussed here. $\Delta$ is defined as $[1 = (n_{cl}/n_0)^2]/2$ The loss $\alpha$ is normalized according to $\alpha\rho^3/[\sigma h(\Delta)]^2$, where $\sigma$ is the RMS diameter variation and $h(\Delta)$ is the correction factor for large index of refraction differences. The three curves represent different values of $2\pi n\rho/\lambda$, where n is the index of refraction of the core, and $\lambda$ is the free space wavelength. For Nd:YAG with $n=1.8$ and $\lambda=1.06\mu m$, the curves correspond to $\rho$ =25, 50 and 100μm. Two general trends can be extracted from this graph for $0.02<D/\rho<20$. First, the losses scale as $\rho^{-3/2}$, in agreement with experimental observations for the unclad open-loop fibers. Second, the loss depends only on $(D/\rho)^{1/2}$, so that small errors in estimating this parameter do not seriously affect the results. Losses calculated according to the fit to the data, Eq. 4.1, are plotted on Fig. 4.1, and can be seen to fall close to the theoretical curves. The loss for the unclad closed-loop fiber is also plotted in Fig. 4.1, and is again seen to fall on the theoretical curves.

Now consider Fig 4.2, which plots normalized loss calculated as a function of normalized autocorrelation length $D/\rho$ for a fixed normalized radius of $2\pi n\rho/\lambda = 267$. This normalized radius corresponds to 50μm diameter at 1.06μm wavelength. The two curves are for different values of the profile height $\Delta$, appropriate for unclad and cladded Nd:YAG fibers. The normalized curves are indistinguishable over the range of $D/\rho$ of interest, so the dependence of loss on cladding index is only through $h(\Delta)$. The loss of the clad 41μm diameter fiber can be compared to that of the 48μm unclad fiber using the $\sigma^2 h(\Delta)^2 \rho^{-3/2}$ scaling given previously. The loss of the unclad fiber is predicted to be 1.5 times larger than that of the clad fiber, compared to the experimentally observed factor of 3.

The above results indicate that the simple correlations predicted by theory are able to scale the losses for a factor of 5 variation in radius, a factor of 12 in index profile depth, and a factor of 5 in RMS diameter variation. The experimental data are uncertain by factors on the order of two, so that the accuracy of the theoretical predictions can be taken to agree with experiments only within this limit. However, given the large range of parameters over which the fits are reasonable, the theory can be regarded as correctly reproducing the essential dependencies.

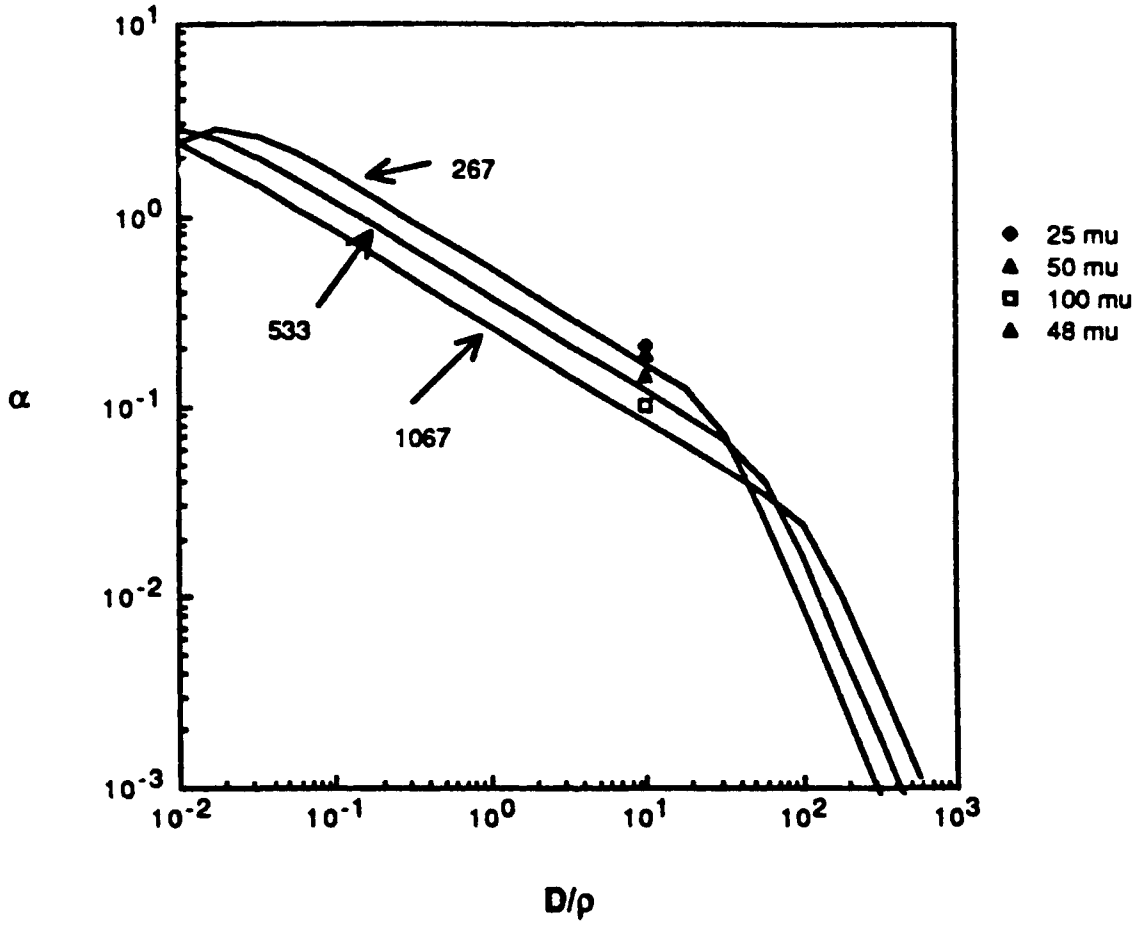


Figure 4.1. Mode-coupling loss normalized to $\sigma^2h^2/\rho^3$ vs. the normalized autocorrelation length. (Curves labled with the value of $2\pi m\rho/\lambda$)

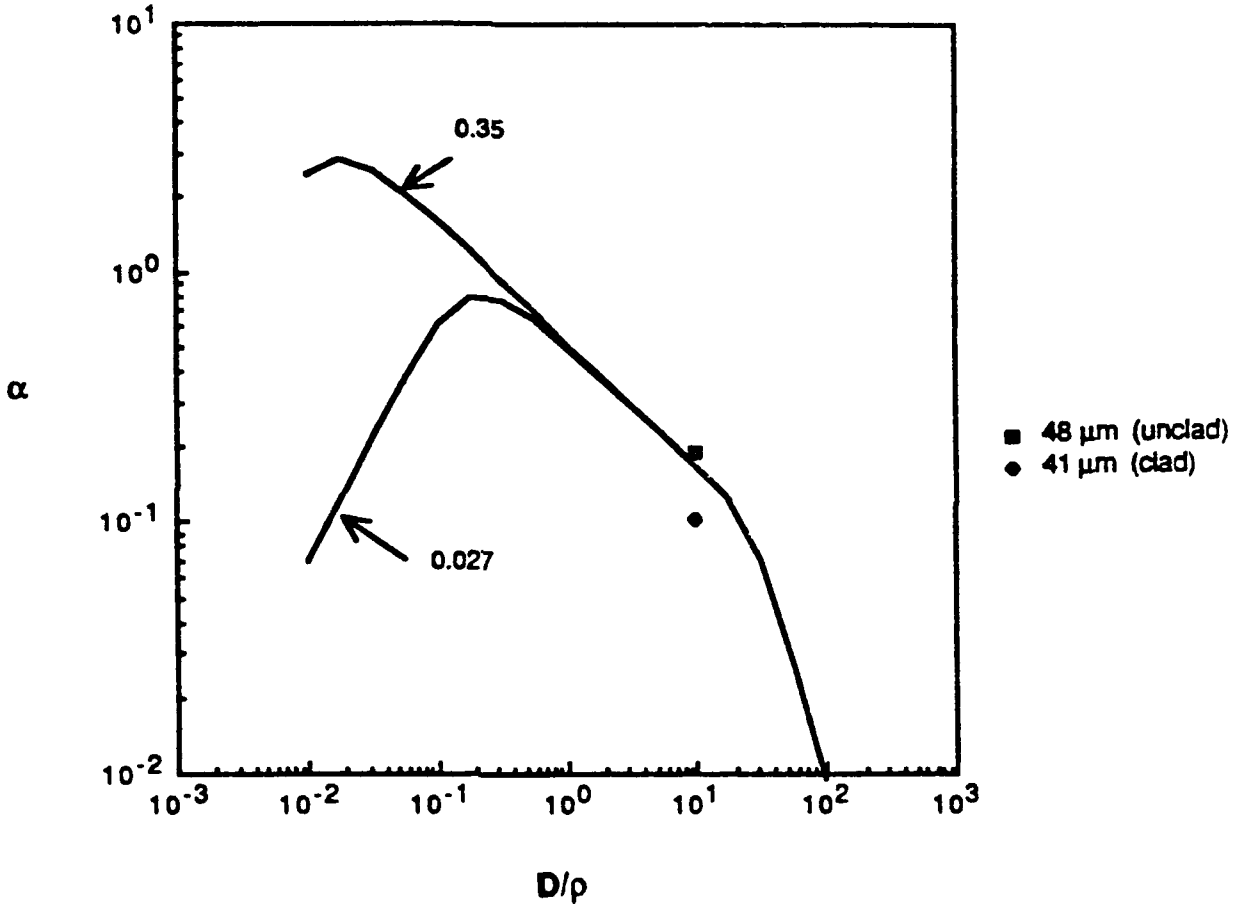


Figure 4.2. Mode-coupling loss normalized to $\sigma^2h^2/\rho^3$ vs. the normalized autocorrelation length at a fixed ratio of fiber radius to wavelength.

b. Radiation Losses

Guided-mode coupling, discussed in the previous subsection, is the loss mechanism of primary importance in nonlinear devices, where light removed from the fundamental mode is essentially lost to the interaction. For power transmission applications, one is less interested in the distribution of the energy among the modes than the power that actually leaks from the fiber. Thus, even though the coupling to radiation modes is expected to be smaller than that to guided modes for fibers whose diameter variations have narrow power spectra, the radiation losses are important in these passive applications.

The coupling between the fundamental mode and radiation modes is dictated by the high spatial frequency components of the diameter variations. Since these components are general small, this coupling is expected to be weak. It is difficult to formulate the theory of such interactions, because of the complexity of the radiation modes of a fiber whose index difference is not small. Such a calculation may be incorrect in principle anyway, because the primary coupling to radiation modes may not be from the fundamental mode, but rather through a "ladder" excitation, where light from the fundamental mode scatters into higher order guided modes, which in turn couple more strongly to the radiation modes than does the fundamental mode. Thus it is likely the dominant mechanism when direct coupling is strongly suppressed. The analysis in this case is complex, so that it is difficult to estimate the radiation losses, but a significant fraction of the light lost to higher order guided modes may well leak out of the fiber. One consequence of such a higher order loss mechanism would be a length-dependent radiation loss coefficient, as the loss would depend on the mix of guided modes present in the fiber. A length-resolved loss measurement would be necessary to determine the dominant loss mechanism, but this has not been done as yet.

Scattering loss measurements have been made by a method described in detail in Ref. 4. The results obtained at Stanford for two unclad 170μm diameter sapphire fibers are shown in the Fig. 4.3. One of the fibers was grown without feedback control of the diameter, while the other was grown with closed loop control. Their RMS diameter variations are 2% and 0.2% respectively. The losses are quite small, on the order of $10^{-3}$dB/cm, and are approximately inversely proportional to the wavelength. The lowest loss, measured at 3.39μm, is equivalent to 80 dB/km, comparable to the losses obrtained in early glass fibers. The loss coefficient of the diameter controlled fiber is the same or slightly larger than that of the open-loop fiber. This can be explained by the characteristic spatial frequencies of the diameter variations in the closed-loop fiber which are higher than those in the open-loop fibers and which would enhance the coupling to radiation modes in the closed-loop fibers.

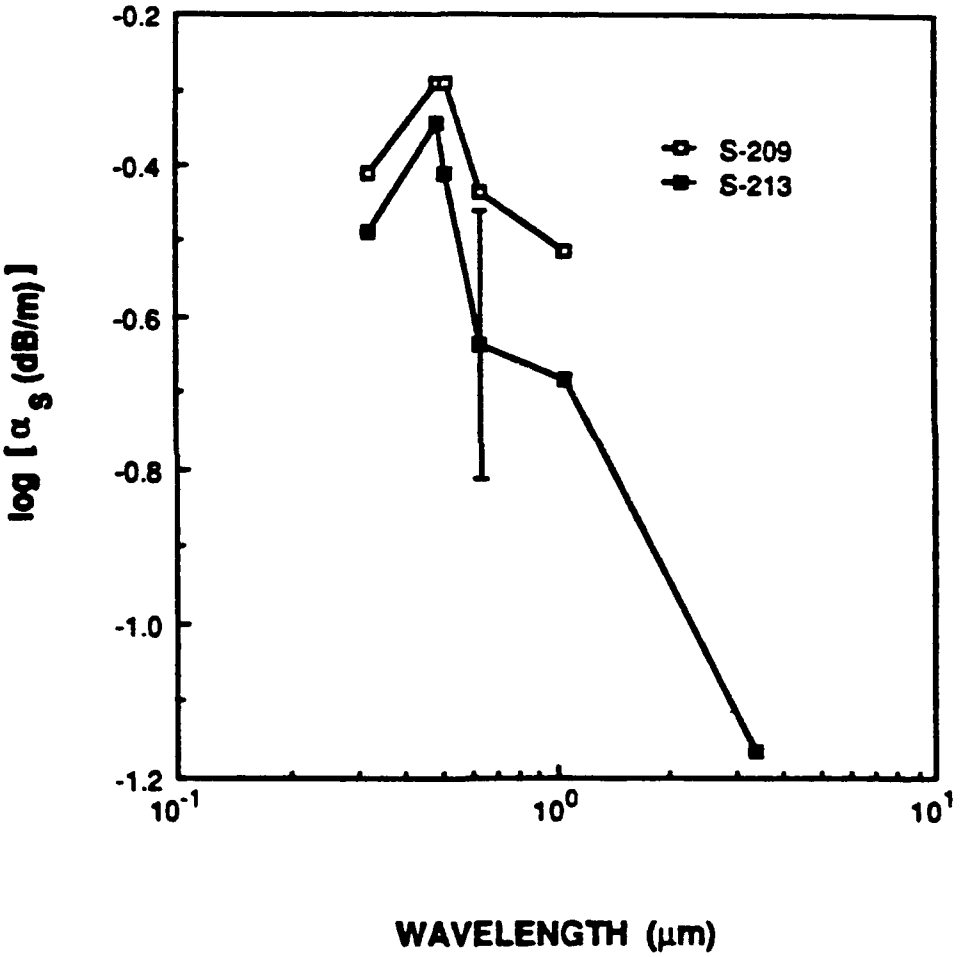


Figure 4.3. Radiation loss in dB/m vs. wavelength for two unclad sapphire fibers

c. Absorption Losses

The absorption losses in single crystal fibers should be similar to those int he starting rod from which the fiber is grown. For most materials, the problem of producing fibers with low absorption losses thus reduces to the problem of finding sufficiently pure starting material. Exceptions to this rule include materials containing a volatile component, in which case the fiber could have a different composition than the source, and materials that partially decompose on melting. For most materials of interest in device applications, the absorption is small compared to the losses due to guided mode coupling.

The measurement of absorption losses by a direct insertion loss measurement is not appropriate for materials with an absorption that is less than $0.001 cm^{-1}$, because of the difficulty in separating the small reduction in throughput due to absorption from the much larger reduction due to reflection. The simplest technique is vacuum calorimetry. In this method, the sample is illuminated with a laser beam at the wavelength of interest, and the temperature rise is measured as a function of time. The temperature rise can be related through simple heat transfer calculations to the amount of power deposited in the fiber, from which the absorption coefficient can be extracted if the incident laser power is known.

For a cylindrical rod, the relation between the absorption coefficient and the temperature rise is:

$$\alpha = \pi D h \Delta T / P \qquad 4.2$$

where $\alpha$ is the absorption coefficient, D is the diameter of the fiber, H is the coefficient of heat loss from the surface of the fiber, $\Delta T$ is the temperature rise, and P is the incident laser power. H may be calculated theoretically, or extracted from the exponential decay of the temperature along the length of a fiber heated at one end. Using the latter method, it is found that for $Al_2O_3$ rods in air, $h \approx 1 mW/Kcm^2$, while in vacuum $h \approx 0.3 mW/Kcm^2$. For a 500 mm diameter rod we have that.

$$\alpha(cm^{-1}) = 0.16 \Delta T(°K)/P(mW) \qquad 4.3$$

Stanford has measured the absorption coefficient in "craquelle" sapphire source material.[42] At 515nm, the absorption is $1 \times 10^{-3} cm^{-1}$. The losses measured in fibers grown from this material are similar to those for the source, as would be anticipated from the previous discussion. We see that the absorption and radiation loss coefficients (Fig. 4.3) are comparable, so both effects must be considered.

LaserGenics, in a program supported by the Army Materials Technology Laboratory, has developed an extremely sensitive vacuum calorimetry technique

which is applicable to any optical material as well as optical fibers. We have applied the technique to over 30 samples of $LiNbO_3$ which have been grown by Crystal Technology Inc. and have demonstrated a sensitivity for the measurement of the absorption coefficient of better than $0.0003\ m^{-1}$.

d. Results

The objective of this single-crystal fiber research is the demonstration of efficient nonlinear optical devices. As is established in the previous sections, nonlinear optical devices require fibers meeting stringent material, structural and processing criteria. The mode confinement of guided wave structures is useful in improving the mode overlap with poor quality pump sources, for reducing the threshold in low-gain materials for such nonlinear devices as optical parametric oscillators, and in producing very high gains for optical conversion.

The scatter losses measured in fiber lasers have been shown to be in qualitative agreement with the predictions of Section 2. Therefore, we can have confidence in the use of these results to predict losses in nonlinear devices. In particular, it has been established that it is possible to propagate a single mode in highly multimoded structures, even without the benefit of a low index of refraction cladding. An example of the output mode of an early unclad monolithic Nd:YAG fiber laser[20] is shown in Fig. 4.4. We see that the profile is close to gaussian. More recent results[41] have shown more than 90% of the output power in the fundamental mode, and losses on the order of $0.01 cm^{-1}$. This level of performance is adequate for some interesting nonlinear devices.

The work on $LiNbO_3$ fibers has focussed on the growth, poling, cladding, and characterization studies. Nonlinear interactions in $LiNbO_3$ fibers have been limited to temperature phasematched second harmonic generation of 532 nm radiation in unclad fibers, with efficiencies comparable to those of bulk interactions in a crystal of the same length.

Early studies of SHG in MgO:$LiNbO_3$ fibers[20] suggested that lithium was lost during growth, presumably through volatilization of $Li_2O$. Carrying out the growth in a wet oxygen atmosphere substantially reduced this problem, but interest in the precise control of the Li/Nb ratio led to investigations of a vapor-phase technique for Li transfer, first suggested by Holman[48] as a means of investigating the phase diagram of $LiNbO_3$. The method involves heating the fiber in the presence of a powder made of a Li-rich mixture of $Li_3NbO_4/LiNbO_3$. The Li vapor in equilibrium with this mixture is absorbed by the lithium-poor fiber until the composition of the fiber reaches the phase boundary between the $LiNbO_3$ and $LiNbO_3 = Li_3NbO_4$. This composition is essentially stoichiometric, i.e., the Li/Nb ratio is close to one. The position of this phase boundary is almost independent of temperature, so the choice of temperature affects only

the rate of the process, not the end result. For Li-poor powders, the phase boundary is temperature dependent, and the composition of the crystal can be controlled by the choice of temperature.

This process has two features of interest. The composition of the crystal is determined by thermodynamic equilibrium, and becomes, in principle, independent of its original composition. Thus, it is possible to produce crystals of very uniform composition, at Li/Nb ratios other than the congruently melting one. Uniform composition is important for efficient nonlinear interactions.

The other important feature is that the birefringence of lithium niobate increases with the Li/Nb ratio. Thus, at a given wavelength, the phasematching temperature increases with Li/Nb ratio, so that one can, for example, produce a composition that phasematches above the annealing temperature for photorefractive damage. Alternatively, at a fixed temperature, the phasematching wavelength decreases, so that it may be possible to phasematch for SHG into the blue at room temperature.

Although one can have some degree of control of the quality and composition of the fiber after the growth of the fiber, it is certainly prefered to be able to grow fibers of high optical quality. From a commercial standpoint, the fewer steps needed to produce a device the better from the stand point of yield and therefore cost. During the course of the program, we made 18 growth runs in our facility of $MgO.LiNbO_3$. The early growth runs were similar to those grown at Stanford University. The fibers exhibited a significant degree of browning and had a high density of defects. As experience was gained in the growth process, the quality of the fibers experienced a marked improvement in optical quality. Towards the end of the program we were able to grow $MgO.LiNbO_3$ fibers of very good optical quality. Some examples of these fibers are shown in Fig. 4.5. Although the optical quality of these fibers was high the mechanical characteristics were still not ideal in that the fibers were still too brittle and therefore too fragile. Annealing the fibers markedly improved the mechanical strength of the fibers but we were not able to eliminate this process step.

Although we were not able to eliminate the annealing process, this process for high quality optical fibers is rather simple. Our biggest disappointment came in the area of poling the fibers to obtain single domain fibers. We were not able to maintain the necessary stability with the asymmetric heating technique at the temperatures required to achieve single domain fibers. We frequently overheated the fiber so that we melted through it. Combining the electric poling with the asymmetric heating technique only complicated the process. The only process that seemed to appear promising was the combination of uniform heating in a reaction tube and electric field poling. We had much better control in this process. The problem with our experiments with this technique was that at this time the furnace we had was only capable of reaching 1100°C, not high enough to get close to the melting point of $MgO.LiNbO_3$ at 1240°C. Since these experiments were done we have purchased a new furnace

capable of reaching 1500°C. We intend to pursue this technique in the future. However it must be noted that careful control of the temperature is required as any asymmetry in the temperature will lead to the distruction of the fiber. Care must also be used in holding the fiber so that the fiber is in close contact with the electrodes. Our approach to this problem was to cut a fine slot in a high temperature dielectric such as sapphire which holds the two high temperature wire electrodes and the MgO:$LiNbO_3$ fiber. We are confident that this technique will succeed after further development.

e. Conclusions

We have found that MgO:$LiNbO_3$ can be grown in fiber form with very good optical quality. Although the mechanical strength is not what is required for the as-grown fibers, the fibers can be strengthened with a rather simple annealing process. The greatest difficulty was encountered in attempting to pole the fibers in order to obtain single domain a-axis fibers. However, a process utilizing both heating and electric field poling does have promise for achieving the single domain fibers required for nonlinear devices.

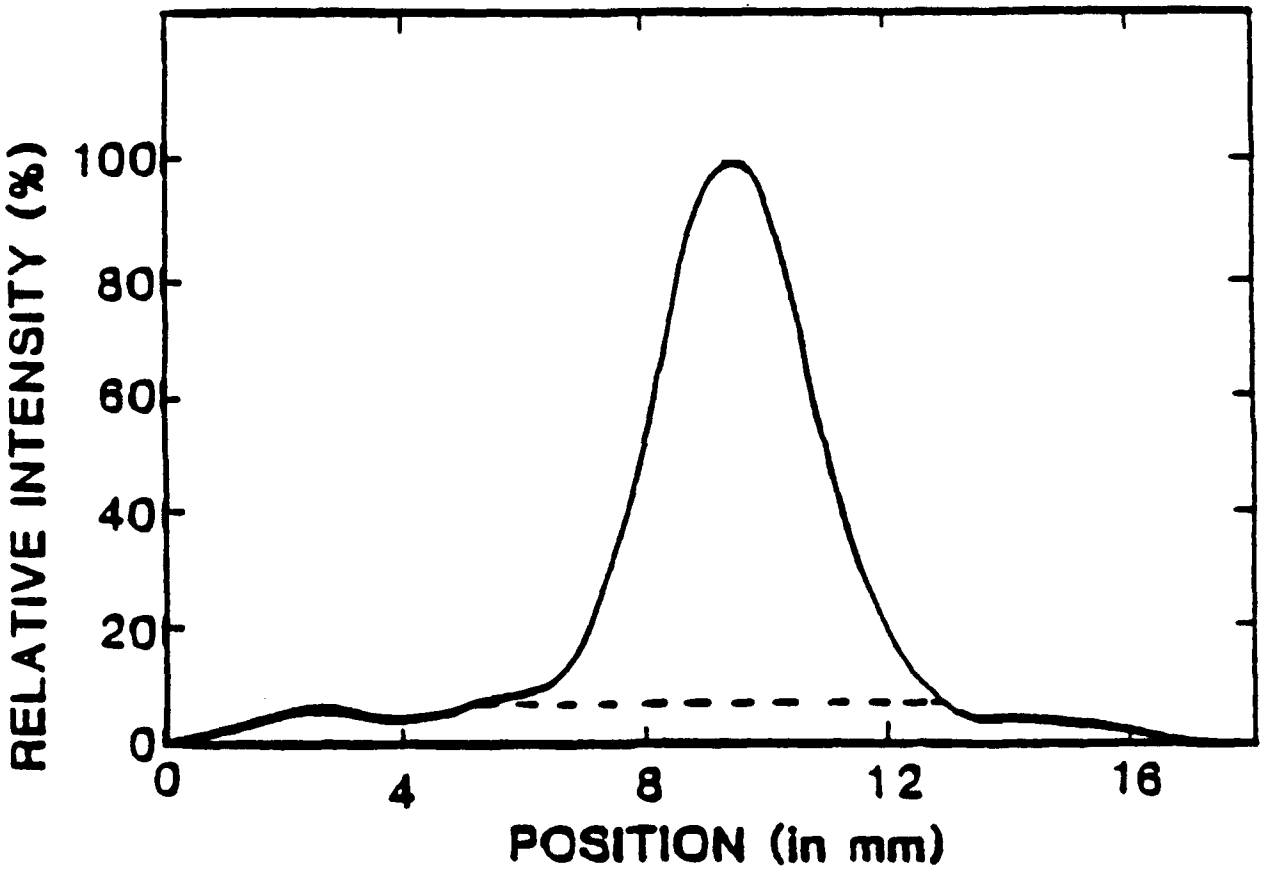


Figure 4.4. Mode profile of an early unclad Nd:YAG fiber laser

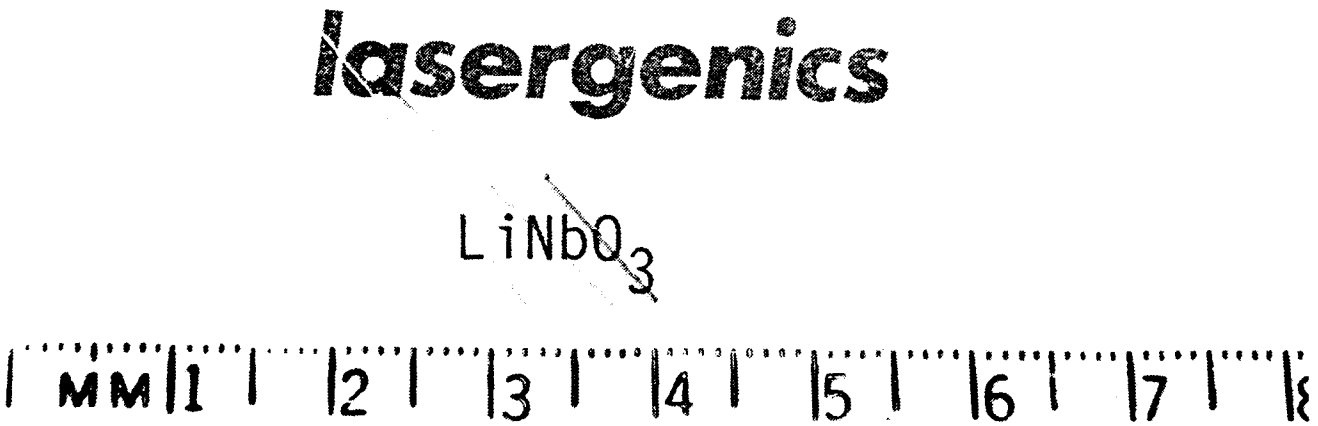


Figure 4.5. Fibers of MgO:$LiNbO^3$ grown by the LHPG technique.

## REFERENCES


1. R. L. Byer, J. F. Young & R. S. Feigleson, J. Appl. Phys. 41, 2320(1970)
2. K. Nassua, H. J. Levinstein & G. M. Loicono, J. Phys. Chem. Solids 27, 933 (1966)
3. J. L. Jackel, D. H. Olson & A. M. Glass, J. Appl. Phys. 52, 4855 (1981)
4. M. E. Lines & A. M. Glass, Principles and Applications of Ferroelectrics and Related Materials, Oxford University Press, New York (1977)
5. M. Fejer, Ph. D. Dissertation, Stanford University (1987)
6. J. A. Armstrong, N. Bloembergen, J. Ducuing, & P. S. Pershan, Phys. Rev. 127, 1918 (1962)
7. D. Marcuse, Theory of Dielectric Optical Waveguides, Academic Press, New York, (1974)
8. D. Marcuse, Bell System Tech. J. 49, 3217 (1969)
9. D. Marcuse, Bell System Tech. J. 49, 1665 (1969)
10. P. Mazur & D. L. Mills, J. Appl. Phys. 54, 3735 (1983)
11. M. Eve & J. H. Hannay, Optics & Quantum Elec. 8, 503 (1976)
12. A. W. Snyder & J. D. Love, Optical Waveguide Theory, Chapman & Hall, New York (1974)
13. D. Gloge, Bell System Tech. J. 51, 1767 (1972)
14. M. C. Vassell, Optics & Quantum Elec. 8, 23 (1976)
15. J. A. Harrington & M. Sparks, Optics Lett. 8, 223 (1983)
16. J. A. Harrington & A. G. Standlee, Appl. Optics 22, 3073 (1983)
17. M. G. Sparks & L. G. DeShazer, Proc. SPIE 266, 3 (1981)
18. R. Olshansky & D. A. Nolan, Appl. Optics 15, 1045 (1976)
19. A. Hadni, J. M. Bassia, X. Gerbaux & R. Thomas, Appl. Optics 15, 2150 (1976)
20. J. L. Nightingale, "The Growth and Optical Applications of Single-Crystal Fibers", Ph.D. thesis, Stanford University (1985)
21. Y. S. Luh, R. S. Feigelson, M. M. Fejer & R. L. Byer, J. Crys. Growth
22. K. Nassau, H. J. Levinstein & G. M. Loiacono, J. Phys. Chem. of Solids 27, 989 (1966)
23. R. R. Turk, "Rolling a KCl fiber. a feasibility study", Proc. SPIE 320, "Advances in Infrared Fibers II", 93-101 (1982).
24. B. Nayar, in Technical Digest of the Topical Meeting on integrated and Guided Wave Optics, (O.S.A. Washington D.C., 1982), paper ThA2.
25. H. E. LaBelle, Mat. Res. Bull. 6, 581 (1971).
26. J. Crystal Growth 50(1), (1980) is entirely devoted to shaped crystal growth, and includes a bibliography complete up to that date
27. Y. Mimura, Y. Okamura, Y Komazawa, and C. Ota, Japanese J. of Appl. Phys. 19, L269 (1980)
28. T. J. Bridges, Optics Lett. 5, 85 (1980).
29. J. S. Haggerty, NASA Cr-120948 (1972)

30. C. A. Burrus and J. Stone, Appl. Phys. Lett. 26, 318 (1975).
31. M. Fejer, J. Nightingale, G. Magel and R. L. Byer, Rev. Sci. Instr. 55, 1791(1984).
32. R. S. Feigelson, "Growth of fiber crystals", Crystal Growth of Electronic Materials, ed. by E. Kaldis, North-Holland, New York, 127-145 (1985).
33. T Fukuda and H. Hirano, J. Cryst. Growth 35, 127 (1976).
34. S. Matsumura and T. Fukuda, J. Cryst. Growth 34, 350 (1976)
35. J. Stone and C. A. Burrus, Fiber and Integrated Optics 2, 19 (1979).
36. U. C. Paek, Appl. Opt. 13, 1383 (1974).
37. J. E Midwinter, Optical Fibers for Transmission, John Wiley & Sons, New York, NY, 194 (1979).
38. W. R. Edmonds, Appl. Opt. 12, 1940 (1973).
39. R. S. Feigelson, W. L. Kway and R. K. Route, Proc. SPIE 484, 133 (1984)
40. J. Stone & C. A. Burrus, J. Appl. Phys. 49, 2281 (1978)
41. M. J. F. Digonnet, c. J. Gaeta, D. O'Meara, and H> J> Shaw, J. Lightwave Tech. LT-5, 642 (1987)
42. Extra Pure Grade Verneuil Craquelle Sappuire, Adolf Meller Co., P. O. Box A6001, Providence, RI 02940
43. R. R. Dils, J. Appl. Phys. 54, 1198 (1983)
44. M. J. F. Digonnet & H. J. Shaw, European Conference on Integrated Optics, Florence, Italy, Oct. 1983
45. J. L. Nightingale & R. L. Byer, Opt. Commun. 56, 41 (1985)
46. M. J F. Digonnet, C. J. Gaeta & H. J. Shaw, J. Lightwave Tech. LT-4, 454 (1986)
47. J. L. Nightingale & R. L. Byer, Opt. Lett.
48. R L. Holman, P. J. Cressman & J. F. Revelli, Appl. Phys. Lett. 32, 280 (1978)